



**HAL**  
open science

# Optimal Energy Storage System-Based Virtual Inertia Placement: A Frequency Stability Point of View

Hêmin Golpîra, Azin Atarodi, Shiva Amini, Arturo Roman Messina, Bruno Francois, Hassan Bevrani

► **To cite this version:**

Hêmin Golpîra, Azin Atarodi, Shiva Amini, Arturo Roman Messina, Bruno Francois, et al.. Optimal Energy Storage System-Based Virtual Inertia Placement: A Frequency Stability Point of View. IEEE Transactions on Power Systems, 2020, 35 (6), pp.4824 - 4835. 10.1109/tpwrs.2020.3000324 . hal-03703454

**HAL Id: hal-03703454**

**<https://hal.science/hal-03703454>**

Submitted on 27 Jun 2022

**HAL** is a multi-disciplinary open access archive for the deposit and dissemination of scientific research documents, whether they are published or not. The documents may come from teaching and research institutions in France or abroad, or from public or private research centers.

L'archive ouverte pluridisciplinaire **HAL**, est destinée au dépôt et à la diffusion de documents scientifiques de niveau recherche, publiés ou non, émanant des établissements d'enseignement et de recherche français ou étrangers, des laboratoires publics ou privés.

# Optimal Energy Storage System-Based Virtual Inertia Placement: A Frequency Stability Point of View

Hêmin Golpîra <sup>1b</sup>, Azin Atarodi, Shiva Amini <sup>1b</sup>, Arturo Roman Messina <sup>1b</sup>, *Fellow, IEEE*,  
Bruno Francois, *Senior Member, IEEE*, and Hassan Bevrani, *Senior Member, IEEE*

**Abstract**—In this paper, the problem of optimal placement of virtual inertia is considered as a techno-economic problem from a frequency stability point of view. First, a data driven-based equivalent model of battery energy storage systems, as seen from the electrical system, is proposed. This experimentally validated model takes advantage of the energy storage system special attributes to contribute to inertial response enhancement, via the virtual inertia concept. Then, a new framework is proposed, which considers the battery storage system features, including annual costs, lifetime and state of charge, into the optimal placement formulation to enhance frequency response with a minimum storage capacity. Two well-known dynamical frequency criteria, the frequency nadir and the rate of change of frequency, are utilized in the optimization formulation to determine minimum energy storage systems. Moreover, a power angle-based stability index is also used to assess the effect of virtual inertia on transient stability. Sensitivity and uncertainty analyses are further conducted to assess the applicability of the method. The efficiency of the proposed framework is demonstrated on a linearized model of a three-area power system as well as two nonlinear systems. Simulation results suggest that the proposed method gives improved results in terms of stability measures and less ESS capacity, when compared with other methods proposed in the literature.

**Index Terms**—Optimal placement, frequency nadir, virtual inertia, energy storage systems, inertial response, rate of change of frequency, transient stability, uncertainty analysis, sensitivity analysis.

## NOMENCLATURE

$\delta^s$	Mechanical rotor angle ( <i>rad</i> )
$\omega^s$	Mechanical rotor angular speed ( <i>rad/s</i> )
$\omega_0$	Rated angular speed ( <i>rad/s</i> )
$T_m(t)$	Mechanical input torque ( <i>p.u.</i> )
$T_e(t)$	Electrical output torque ( <i>p.u.</i> )
$H$	Inertia constant of the system ( <i>s</i> )

Manuscript received January 7, 2020; revised March 30, 2020 and May 26, 2020; accepted May 30, 2020. Paper no. TPWRS-00030-2020. (*Corresponding author: Hemin Golpîra.*)

Hêmin Golpîra, Azin Atarodi, Shiva Amini, and Hassan Bevrani are with the Department of Electrical and Computer Engineering, University of Kurdistan, Sanandaj 66177-15175, Iran (e-mail: hemin.golpira@uok.ac.ir; a.atarodi@eng.uok.ac.ir; sh.amini@eng.uok.ac.ir; bevrani@uok.ac.ir, golpira@wisc.edu).

Arturo Roman Messina is with the CINVESTAV, Guadalajara 21573, Mexico (e-mail: arturo.roman@cinvestav.mx).

Bruno Francois is with the Arts et Métiers Paris Tech, HEI, EA 2697-L2EP, Laboratory of Electrical Engineering and Power Electronics, University of Lille, Centrale Lille 59800, France (e-mail: bruno.francois@centralelille.fr).

Color versions of one or more of the figures in this article are available online at <https://ieeexplore.ieee.org>.

Digital Object Identifier 10.1109/TPWRS.2020.3000324

$h_i$	Inertia of ESS in area $i$ ( <i>s</i> )	39
$h_{i, \min}^i$	Minimum required ESS inertia, in compliance with RoCof, in area $i$ ( <i>s</i> )	40
$h_{i, \min}''$	Minimum required ESS inertia, in compliance with frequency nadir, in area $i$ ( <i>s</i> )	41
$I(t)$	Impulse response of the system	42
$P(n)$	Data sequence of interest	43
$P_{in}$	Injected power of ESS to the host grid	44
$K$	Number of sinusoidal components in noise	45
$L$	Length of $P(n)$	46
$a_k$	Magnitude	47
$\Phi_k$	Initial phase angle	48
$\omega_k$	Harmonic frequency in radius	49
$A_k$	Complex magnitude of the $k$ th-harmonic	50
$s_i$	Eigenvectors associated with the noise subspace	51
$e$	Signal eigenvector	52
$e^U$	Complex-conjugate transpose of $e$	53
$C_{cap}$	Capital costs ( $\$/kW$ )	54
$C_{PCS}$	Power conversion system costs ( $\$/kW$ )	55
$C_{stor}$	Storage section costs ( $\$/kWh$ )	56
$C_{BOP}$	Power balance costs ( $\$/kW$ )	57
$t_{ch}$	Charging /discharging time ( <i>h</i> )	58
$C_{O\&M}$	Operation and maintenance costs ( $\$/kW-yr$ )	59
$C_{R,a}$	Annualized replacement costs ( $\$/kW-yr$ )	60
$C_{cap,a}$	Annualized total capital costs ( $\$/kW-yr$ )	61
$C_{LCC,a}$	Annualized life cycle costs ( $\$/kW-yr$ )	62
$CRF$	Capital recovery factor	63
$C_R$	Replacement costs ( $\$/kWh$ )	64
$C_{FOM,a}$	Fixed operation and maintenance costs ( $\$/kW-yr$ )	65
$C_{VOM,a}$	Variable operation and maintenance costs ( $\$/kW-yr$ )	66
$n_{cycle}$	Number of discharge cycles per year	67
$\zeta_c$	Charging efficiency of the battery (%)	68
$\zeta_d$	Discharging efficiency of the battery (%)	69
$\eta$	Power angle-based stability index	70

## I. INTRODUCTION

**I**NERTIAL response is defined as the power associated with changes in kinetic energy of synchronous generator rotors, in response to frequency changes, which is fed(taken) to(from) the grid [1]. Before reaction of traditional ancillary control loops, this energy, provided by system inertia, is the key factor to limit the power imbalance. System inertia has a major influence on frequency stability and the associated rate of change of frequency (*RoCoF*) and frequency nadir.

Inverter-based renewable sources are increasingly replacing synchronous generators, which in turn decrease overall system inertia. The ever-growing number of frequency incidents, in response to fluctuations of renewable power sources, accompanied with low level inertia feature jeopardize frequency stability [2]–[4]. This motivates the need to develop advanced ancillary energy balancing services to control frequency changes. Paramount among these, is Virtual Inertia emulation which mitigates undesired frequency dynamics. However, not only insufficient level of inertia, but also its heterogeneous distribution together with time-varying inertia profiles may render frequency dynamics faster. These facts, along with the need to economically keep system secure, make optimal placement of virtual inertia a key factor [2]. This paper addresses the problem of optimal placement of virtual inertia in power grids from a fundamentally new perspective.

Effects of energy storage systems (ESSs) on frequency regulation have been studied in recent research works such as [5]–[7]. They deal with balancing of generation and load to maintain a constant system frequency and to keep tie-line power flows at scheduled values. These studies consider long term frequency response as well as steady state metrics, while neglect inertia requirements and primary frequency as the main metrics utilized for system resilience analysis. Some recent studies have investigated the effect of low system inertia on frequency stability [8]–[14]. In parallel with these efforts, recent research works [15]–[21] demonstrate the way on which virtual inertia could be emulated in different ways, including appropriate control of wind turbines and energy storage systems (ESSs). In [22], an optimization framework to deal with various aspects of inertia emulation and control including how inertia emulation impacts system stability, and determining the best places to add virtual inertia is proposed. Some questions about the heterogeneous inertial profiles and how the associated negative impacts are reduced by inertia emulation has been raised in [11]. Poolla et al. [2] and Farmer et al. [19] focus on  $H_2$  performance metric to determine optimal placement of virtual inertia. Determination of the optimum size of battery to provide the primary frequency control is addressed in [23], [24]. In particular, ESSs do not constantly participate in primary regulation, due to life-time concerns. Instead, in practice, the ESSs are controlled in a hierarchical fashion, dispatched by an optimal function to guarantee the State-of-Charge (SOC) and life-time constraints, which is missed in the so far researches. Some research works, such as [25], deal with optimal placement of virtual inertia in power system considering network structure. It employs DC-power flow to tackle network structure into formulation.

A main limitation of these approaches is the reliance on steady state considerations. It is well known, however, that dynamical frequency indices, such as RoCoF and frequency nadir, are important parameters in assessing frequency stability and the activation of protection schemes. This paper re-formulates the virtual inertia placement problem in term of dynamical metrics. Using this approach, the effects of virtual inertia on the frequency indices can be assessed using a dynamic equivalent model obtained by mapping the electromechanical behavior of ESSs onto a second-order synchronous generator (SG) model.

The main contributions of this paper can be summarized as follows:

- An attempt is made to systematically represent the ESS dynamical behavior by a second-order SG model that extends previous work by the authors [15] on the emulation of virtual inertia. Within this framework, a new signal processing technique, called Multiple Signal Classification (MUSIC) algorithm is developed to derive the model.
- As formulating differential equations in the optimization problem is a hard task, a mathematical framework is proposed to represent dynamical metrics by algebraic inequality constraints. In particular, the present paper describes the complex optimization problem of virtual inertia placement by a new simple formulation.
- Since, the ESSs sizing is a difficult problem in practice, and considering the energy capacity, price, life-time and SOC may not be addressed by the proposed synchronous-based model; an attempt is made to tie the virtual inertia to the ESS features.

## II. VIRTUAL INERTIA EQUIVALENT MODEL

### A. General Concept

The main step towards optimal placement of virtual inertia in a power grid is to analyze its effects on the frequency stability behavior. This could be visualized by appropriate modelling of the virtual inertia. Generally, providing virtual inertia and thereby contributing to the overall equivalent grid inertia could be achieved by using the virtual synchronous generator (VSG) concept. VSG relies on similar power-balance-based synchronization mechanism as SGs to realize such functionality [26], which would be investigated for modeling purpose in this paper.

With synchronous generation being displaced with modern power electronic based generation such a solar and wind generation, the analysis of inertial response of variable resource generation becomes of fundamental importance. Energy storage systems can, in principle, provide most of its stored energy to support frequency in an interconnected power system and hence a set of large battery ESSs could play the same role as SGs in the inertial response horizon. Conceptually, the charging/discharging process of ESS can be interpreted as the initial compensation of a disturbance by the stored kinetic energy of a SG rotating mass. This means that, while the ESSs would be triggered by a command signal, from frequency measurements, for charging/discharging, a SG model could be used to represent the associated dynamics.

The classical model of a SG is a second-order model of the form

$$\begin{cases} \dot{\delta}^s = \omega^s(t) - \omega_0 \\ H\dot{\omega}^s = T_m(t) - T_e(t) \end{cases} \quad (1)$$

where  $\delta^s$ ,  $\omega^s$ , and  $\omega_0$  are the mechanical rotor angle, the mechanical rotor angular speed and the initial angular speed, respectively;  $H$ ,  $T_m(t)$  and  $T_e(t)$  are the inertia constant, mechanical input torque and electrical output torque, respectively [27].

189 Taking the slow electromechanical behavior of the battery  
 190 ESS into account, the associated dynamics could be represented  
 191 by (1). The problem of interest, however, is to calculate the  
 192 equivalent inertia constant and mechanical input torque. To deal  
 193 with this possibility, a data-driven approach in which uncertain  
 194 behavior of the ESS is inherently considered to provide comple-  
 195 mentary information for the swing equation model of (1), is  
 196 proposed.

197 **B. Data Driven-Based Equivalent Model:** To introduce the  
 198 proposed equivalent model, assume that the injected power of the  
 199 ESS to the host grid is a discrete-time signal  $P(n)$  of length  $L$ . Let  
 200 the time-varying signal  $P(n)$  be decomposed into  $K$  sinusoidal  
 201 components in noise, as [28], [29]:

$$P(n) = \sum_{k=1}^K a_k \cos(n\omega_k + \Phi_k) + w(n) \quad (2)$$

202 where,  $a_k$ ,  $\Phi_k$ ,  $\omega_k$  and  $w(n)$  are the magnitude and the initial  
 203 phase angle, harmonic frequency in radius and additive white  
 204 noise, respectively. In the model,  $a_k$  and  $\omega_k$  are assumed to be  
 205 deterministic and unknown, and  $\Phi_k$  is unknown and assumed to  
 206 be random and uniformly distributed in  $[-\pi, \pi]$ . Alternatively,  
 207 the model (2) can be expressed in the form of noisy complex  
 208 exponentials as [19]

$$P(n) = \sum_{k=1}^K A_k e^{jn\omega_k} + w(n) \quad (3)$$

209 where  $A_k = |A_k|e^{j\Phi_k}$  is the complex magnitude of the  $k$ th-  
 210 harmonic(noise) signal component. As the MUSIC algorithm  
 211 is a noise subspace-based method, it is a good tool to deal with  
 212 experimental noisy measured signals. Using this framework, the  
 213 dimensional space is divided into signal and noise components,  
 214 which is of high importance to accurately calculate  $H$  and  $T_m(t)$   
 215 in (1).

216 The MUSIC method employs a harmonic model and estimates  
 217 the frequencies and powers of the harmonics in the signal.  
 218 Application of the MUSIC method to the data sequence,  $P(n)$ ,  
 219 gives:

$$P_{MUSIC}(e^{j\omega}) = \frac{1}{\sum_{i=K+1}^M |e^U s_i|^2} \quad (4)$$

220 where the  $s_i$  are the eigenvectors associated with the noise  
 221 subspace that are orthogonal to the signal eigenvector  $e =$   
 222  $[1 e^{j\omega} e^{j2\omega} \dots e^{j(M-1)\omega}]^T$ , and  $e^U$  denotes the complex-conjugate  
 223 transpose;  $M$  is the dimension of space spanned by  $P(n)$ . It is  
 224 worth emphasizing that  $P_{MUSIC}(e^{j\omega})$  in (4) does not relate to  
 225 any real power spectrum; rather, the only purpose of this pseudo-  
 226 spectrum is to generate peaks whose frequencies correspond  
 227 to those of the dominant frequency components. This feature  
 228 makes the MUSIC approach interesting to develop equivalent  
 229 model based on dominant modes.

230 For a given signal of interest and according to (2)–(4), eigen-  
 231 values would be calculated. By knowing the eigenvalues and  
 232 because the impulse response is the inverse Laplace transform  
 233 of eigenvalues, one could represent a signal of interest with

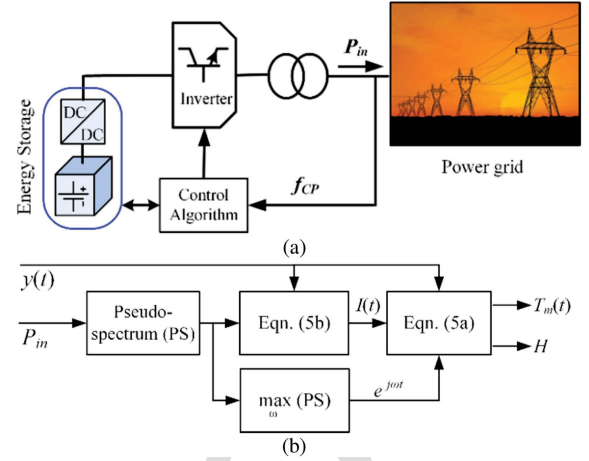


Fig. 1. Block diagram representation of the proposed modeling process: (a) virtual inertia emulation mechanism, and (b) the proposed equivalent model;  $P_{in}$ ,  $y(t)$  and  $f_{cp}$  represent the grid injected power, the frequency deviation of the ESS, and the frequency at the point of connection of the ESS, respectively.

a pre-defined model of (1). For this purpose, suppose the im- 234  
 pulse response of system is  $I(t)$ ; for the input signal  $x(t)$ , i.e. 235  
 $x(t) = T_m(t)$  in (1), one could write  $y(t)$ , i.e.  $\dot{\omega}$ , as: 236

$$y(t) = x(t) \int_{t=0}^{\infty} I(t) e^{j\omega t} dt \quad (5.a)$$

where, 237

$$I(t) = y(t) * PS \quad (5.b)$$

and  $PS$  in (5.b) is the pseudo-spectrum of the signal. Equation, 238  
 (5.b) reveals that  $I(t)$  results from convolution of  $y(t)$  and  $PS$ . 239

In the modelling procedure and by measuring the output 240  
 response of the system  $y(t)$  and by knowing  $I(t)$ , the problem 241  
 of interest is to calculate  $x(t)$  in (5). By calculating  $T_m(t)$ , the 242  
 ESS could be replaced by the synchronous generator model of 243  
 (1). Using this approach,  $\omega$  in (5.a) is defined as the dominant 244  
 frequency components of the pseudo-spectrum in (4). 245

Figure 1 gives a schematic illustration of this model. In this 246  
 plot, Fig. 1(a) illustrates the process of virtual inertia emulation 247  
 using the battery ESS, while Fig. 1(b) describes a simplified 248  
 block diagram representation of the proposed equivalent model. 249  
 The input to the control algorithm is the frequency at the con- 250  
 nection point of the inverter  $f_{cp}$ , and  $P_{in}$  represents the grid 251  
 injected power. 252

**C. Model Validation:** The efficiency of the proposed method 253  
 is illustrated using the existing battery ESS in the University of 254  
 Kurdistan Micro-Grid (UOK-MG). Fig. 2 shows a three-phase 255  
 diagram representation of the UOK-MG. Details of the physical 256  
 UOK-MG are given in [30]. 257

Figure 3 shows the battery ESS and the main grid power 258  
 variation behavior, i.e.  $P_{in}$  in Fig. 1, recorded for the UOK-MG. 259  
 As shown in Fig. 3, Event 1 triggers the charging process of the 260  
 ESS in response to deviations from the minimum SOC. 261

The main grid power deviation during the charging process in 262  
 Fig. 3 is utilized to calculate the Pseudo-spectrum (see Fig. 4) 263  
 which, in turn, is used to estimate the dominant frequency 264  
 components in (4). 265

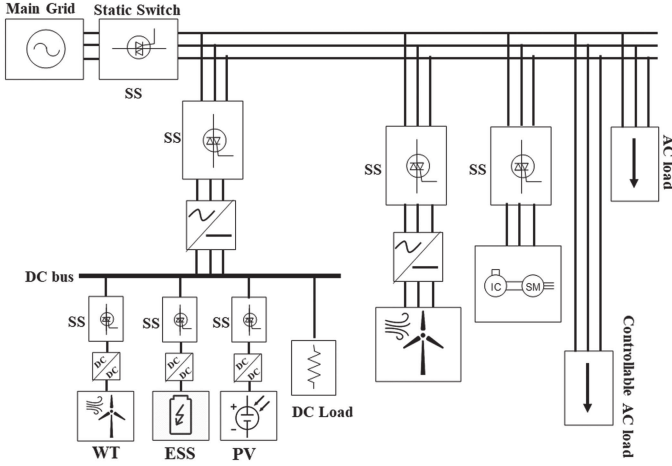


Fig. 2. Three-phase schematic representation of the UOK-MG.

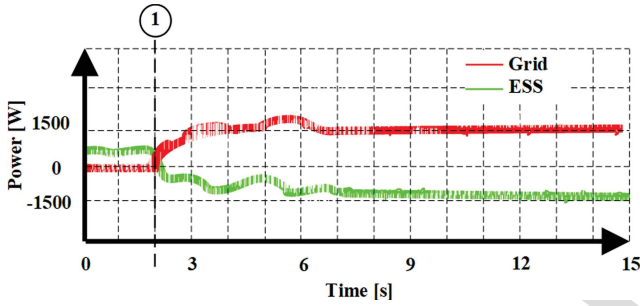


Fig. 3. The ESS and grid experimental dynamic responses.

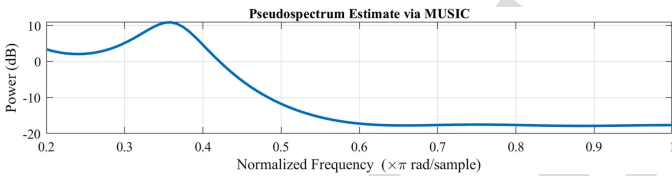


Fig. 4. The Pseudospectrum estimation via MUSIC.

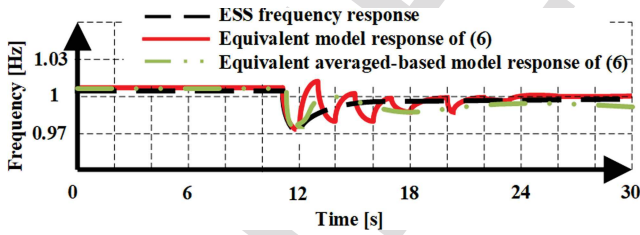


Fig. 5. Comparison of frequency response computed from the experiment and the equivalent frequency response models.

Setting the frequency deviation of the ESS in Fig. 5 as  $y(t)$  and the Pseudo-spectrum of Fig. 4 as  $PS$  for (5) gives:

$$\left\{ \begin{array}{l} \dot{\delta}^s = \omega^s - \omega_0 \\ 0.53\omega^s = (1 - e^{-0.38t}) C - T_e(t) \end{array} \right\} \quad (6)$$

where,  $C$  is a constant value and would be set to fit the DC term in (4). In interpreting this model, note that constant 0.38 in (6) represents the dominant frequency of the Pseudo-spectrum in Fig. 4

which would be fed to (5) to calculate the 0.53 s inertia constant in (6). Figure 5 demonstrates the effectiveness of the equivalent model (6) to approximate the inertial response behavior of the ESS. To exactly mimic frequency behavior of ESS using (6), the oscillatory behavior of the adopted model would be removed using a 20-samples rolling-averaging window. This approach averages the long-term oscillations, and hence, mitigates the oscillatory behavior beyond the inertial response horizon.

Results in Fig. 5 show that the dynamic behavior of ESS, especially in the inertial response horizon can be approximated by a simple SG model. It should be emphasized that while a conventional SG is slower and less flexible compared to ESS, developed dynamical equivalent model of ESSs in the grid connected mode is not only affected by the fast-inherent features of ESSs but also is significantly influenced by the external zone, i.e. the host grid, features.

### III. OPTIMIZATION PROBLEM

This section formulates the ESS placement as an optimal techno-economic problem.

#### A. Costs of Energy Storages and Technologies

There are two main approaches for assessing the cost of storage technologies: 1) Total Capital Cost (TCC), and 2) Life Cycle Cost (LCC) [31]. For the sake of generality of the method, no specific ESS technologies are considered in this section.

In the TCC approach, all terms associated with the purchase, installation, and delivery of the ESS units, including Power Conversion System (PCS) costs ( $C_{PCS}$ ), costs of ESS ( $C_{stor}$ ), and cost of balance of plant ( $C_{BOP}$ ), are considered as:

$$C_{cap} = C_{PCS} + C_{BOP} + C_{stor} \times t_{ch} \quad (\$/kW) \quad (7)$$

where  $t_{ch}$  is the charging /discharging time. The balance of the ESS, known as the BOP, includes site wiring, interconnecting transformers, and other additional ancillary equipment and is measured on a  $\$/kW$  basis [32].

However, the LCC is a more common metric to evaluate and compare different ESS technologies. The annualized LCC is formulated according to (8) which considers operation and maintenance costs ( $C_{o\&M,a}$ ), replacement cost ( $C_{R,a}$ ) and annualized TCC.

$$C_{LCC,a} = C_{cap,a} + C_{o\&M,a} + C_{R,a} \quad (\$/kW - yr) \quad (8)$$

in which:

$$CRF = \frac{i(1+i)^T}{(1+i)^T - 1} \quad (9)$$

$$C_{cap,a} = TCC \times CRF \quad (\$/kW - yr) \quad (10)$$

$$C_{o\&M,a} = C_{FOM,a} + C_{VOM,a} \times n_{cycle} \times t_{ch} \quad (\$/kW - yr) \quad (11)$$

$$C_{R,a} = CRF \times \sum_{k=1}^r (1+i)^{-kt} \times \left( \frac{C_R \times t_{ch}}{\eta_{sys}} \right) \quad (\$/kW - yr) \quad (12)$$

where  $CRF$ ,  $i$ ,  $T$ ,  $r$ ,  $t$ , and  $\eta_{sys}$  are the capital recovery factor, interest rate and the life time, the number of substitutions in lifetime, the replacement period and the overall efficiency, respectively;  $C_{FOM,a}$  and  $C_{VOM,a}$  define the fixed and variable operation and maintenance costs. Subscript “a” stands for “annualized” costs.

### B. Formulation of Objective Function and Constraints

Equation (8) specifies the annual cost per kilowatt of the installed ESS in compliance with the lifetime. However, for optimal placement of virtual inertia, it is necessary to rewrite the cost function in (8) according to the amount of virtual inertia.

The synchronous inertia constant ( $H$ ) is defined as the ratio of stored kinetic energy to the rated apparent power of the system, as:

$$H = \frac{0.5J_{VI} \omega^2}{S_{base}} \quad (13)$$

where  $J_{VI}$ ,  $\omega$ , and  $S_{base}$  are the moment of inertia, angular velocity and rated apparent power, respectively. Since the stored energy in ESSs is usually expressed in volt ampere hour ( $VAh_{ESS}$ ), it is needed to express the associated value in term of Joule. Considering unity power factor, one could re-write (13) as:

$$KW_{ESS} = KVA_{ESS} = \frac{h_{ESS} S_{base}}{3600 \text{ s}} \rightarrow h_{ESS} = \frac{3600 VAh_{ESS}}{S_{base}} \quad (14.a)$$

This equation gives the average hourly power that can be injected/absorbed to/from the grid by the ESS. To validate such representation, results obtained from (14.a), for frequency response of Fig. 5, are compared with those of well-established methods of calculating inertia. Using the classical swing equation during 500 ms after fault occurrence, one can conventionally calculate inertia constant as [33]:

$$H_{Conv.} = \frac{\Delta P_L}{2RoCoF_{500ms}} = \frac{\Delta P_L}{2 \left( \frac{f(0.5) - f(0)}{0.5} \right)} \quad (14.b)$$

A comparison with the frequency responses of Fig. 5 shows an error of 3.17% which in turn justifies the proposed formulation in (14.a).

By substituting (14.a) into (8), one could write the optimization problem as:

$$\text{minimize}_{h_i} F(h_i) = \sum_{i=1}^{n_{ESS}} \left( C_{LCC,a} \times \frac{h_i S_{base}}{3600 \text{ sec}} \right) \quad (15.a)$$

$$\text{st : } RoCoF_i \leq RoCoF_{max} \quad (15.b)$$

$$\Delta f_{nadir \ i} \leq \Delta f_{nadir \ max} \quad (15.c)$$

$$SOC_{min} \leq SOC_i \leq SOC_{max} \quad (15.d)$$

where  $n_{ESS}$  is the number of ESSs. Moreover, the SOC should remain within an appropriate range which is addressed in (15.d).

The SOC can be calculated as follows [34, 35]

$$SOC(\Delta t) = SOC(0) - \frac{\int_0^{\Delta t} \zeta p(t) dt}{E_{ESS, rated}} \quad (16.a)$$

where,

$$\zeta = \begin{cases} \zeta_c & P(t) < 0 \\ \frac{1}{\zeta_d} & P(t) > 0 \end{cases} \quad (16.b)$$

and  $p(t)$  is battery power which gets negative values for the charging procedure and positive values for the discharging period;  $E_{ESS, rated}$ ,  $\Delta t$ ,  $\zeta_c$ , and  $\zeta_d$  are the nominal energy capacity, charge/discharge time, charging and discharging efficiencies of the battery, respectively.

### C. Determining the Bounds of Virtual Inertia

Constraints (15.b) and (15.c) explain that the optimization problem (15) enforces the RoCoF and frequency nadir in all areas to be less than standard values. These terms make the optimization problem difficult to deal with as it depends on dynamical indices. Generally, it is common to specify the lower/upper bounds based on different criteria, including capacity of equipment or budget. Therefore, the problem of interest here is to re-write the upper and lower bounds of (15.b) and (15.c) in terms of the emulated inertia, i.e.  $h$ .

1) *Rate of Change of Frequency*: The RoCoF is a meaningful criterion to show ability of a system in the face of a sudden power imbalance. Greater RoCoF means that the less time is available for system operator to arrest frequency decline [36]. Time interval of 100 milliseconds to 2 seconds are defined to measure the RoCoF [36], [37]. ENTSO standard [37] explains that RoCoF is allowed to get a value between 0.5 to 1 Hz/sec.

In order to represent dynamical frequency indices based on lower bounds of inequality constraints of (15.b), the RoCoF would be defined based on the classical swing equation of (1) as [30]:

$$2H \frac{d\Delta f(t)}{dt} = \Delta P_m(t) - \Delta P_L(t) - \Delta P_{tie}(t) \quad (17)$$

Where  $\Delta P_m(t)$ ,  $\Delta P_L(t)$ , and  $\Delta P_{tie}(t)$  represent mechanical power, electrical power and tie line power changes, respectively. Considering the definition of RoCoF, one could write:

$$RoCoF = \frac{\Delta P_m(t) - \Delta P_L(t) - \Delta P_{tie}(t)}{2H} \quad (18)$$

The Taylor series expansion of (18) about the independent variables of  $H$ ,  $\Delta P_m$ ,  $\Delta P_L$ , and  $\Delta P_{tie}$  gives

$$\begin{aligned} \Delta RoCoF_i &= \frac{\partial RoCoF_i}{\partial \Delta P_{mi}} \Delta \Delta P_{mi} + \frac{\partial RoCoF_i}{\partial \Delta P_{Li}} \Delta \Delta P_{Li} \\ &+ \frac{\partial RoCoF_i}{\partial \Delta P_{tiei}} \Delta \Delta P_{tiei} + \frac{\partial RoCoF_i}{\partial \Delta H_i} \Delta H_i = \frac{1}{2H_i} \Delta \Delta P_{mi} \\ &+ \frac{-1}{2H_i} \Delta \Delta P_{Li} + \frac{-1}{2H_i} \Delta \Delta P_{tiei} \\ &+ \frac{-(\Delta P_{mi} - \Delta P_{Li} - \Delta P_{tiei})}{2H_i^2} \Delta H_i \end{aligned} \quad (19)$$

376 Due to the slow inherent of dynamics of interest, except for the  
377 last term of (19), other terms could be neglected. Accordingly,  
378 and by replacing (18), one could re-write (19) as:

$$RoCoF_i \left( -\frac{\Delta H_i}{H_i} \right) = \Delta RoCoF_i \quad (20)$$

379 Considering maximum allowable RoCoF, i.e.  $RoCoF_{i,max}$ ,  
380 the minimum inertia which guarantees the RoCoF to be within  
381 the permitted range is calculated as:

$$\begin{aligned} h'_{i,min} &= \Delta H_{i,min} \\ &= H_i \left( -\frac{\Delta RoCoF_{i,max}}{RoCoF_i} \right) \xrightarrow{\Delta RoCoF_{i,max} = RoCoF_{i,max} - RoCoF_i} \\ h'_{i,min} &= H_i \left( -\frac{RoCoF_{i,max} - RoCoF_i}{RoCoF_i} \right) \end{aligned} \quad (21)$$

382 where,  $h'_{i,min}$  represents the minimum, in compliance with the  
383 RoCof, required inertia which should be emulated by the battery  
384 ESS in area  $i$ . It equals to the difference between the desired  
385 inertia to enforce system to follow the standards and the present  
386 inertia constant, i.e.  $\Delta H_{i,min}$ .

387 2) *Frequency Nadir*: Frequency nadir mainly depends on the  
388 total inertia of the system and the capability of the power re-  
389 sources to provide primary frequency response [38]. According  
390 to NERC and the Union for the Coordination of the Transmission  
391 of Electricity (UCTE) standards [39, 40], the minimum allow-  
392 able frequency that a system could instantaneously experience  
393 during the operation is 800 mHz.

394 Taking the time dependency of the governor response into  
395 account, one can write the frequency nadir as [15]:

$$\Delta f_{nadir} = \frac{(\Delta P_L + \Delta P_{tie})^2 T_d}{4HR} \quad (22)$$

396 where  $R$  is the extra power received through the governor and  
397  $T_d$  is the response time of the governor. In deriving (22), it  
398 is assumed that the mechanical power through the governor  
399 increases as a linear function of time with the steady gradient  
400  $R/T_d$  [41, 42]. While, this is a conservative assumption, Great  
401 Britain and Ireland practices show that this is the case for the  
402 power increment within 5 and 10 seconds ( $T_d$ ), respectively,  
403 following a contingency [43]. Applying Tayloras expansion to  
404 (22) gives

$$\begin{aligned} \Delta \Delta f_{nadir,i} &= \frac{\partial \Delta f_{nadir,i}}{\partial \Delta P_{Li}} \Delta \Delta P_{Li} + \frac{\partial \Delta f_{nadir,i}}{\partial \Delta P_{tie,i}} \Delta \Delta P_{tie,i} \\ &+ \frac{\partial \Delta f_{nadir,i}}{\partial \Delta H_i} \Delta H_i = \frac{(\Delta P_{Li} + \Delta P_{tie,i}) T_d}{2H_i R_i} \Delta \Delta P_{Li} \\ &+ \frac{(\Delta P_{Li} + \Delta P_{tie,i}) T_d}{2H_i R_i} \Delta \Delta P_{tie,i} \\ &+ \frac{-(\Delta P_{Li} + \Delta P_{tie,i})^2 T_d}{4H_i^2 R_i} \Delta H_i \end{aligned} \quad (23)$$

Following the same procedure as that in (21), one could re-  
write (23) in the form

$$\Delta f_{nadir,i} \left( -\frac{\Delta H_i}{H_i} \right) = \Delta \Delta f_{nadir,i} = \Delta (f_{nadir,i} - f_0) \quad (24)$$

The minimum inertia, i.e.  $h''_{i,min}$ , which guarantees frequency  
nadir to be in the permitted range is calculated by:

$$\begin{aligned} h''_{i,min} &= \Delta H_{i,min} = H_i \left( -\frac{\Delta \Delta f_{nadir,i,max}}{\Delta f_{nadir,i}} \right) \\ &= H_i \left( -\frac{f_{nadir,max} - \Delta f_{nadir,i}}{\Delta f_{nadir,i}} \right) \end{aligned} \quad (25)$$

where,  $h''_{i,min}$  represents the minimum, in compliance with  
frequency nadir, required inertia which should be emulated by  
the battery ESS in area  $i$ . In order to simultaneously satisfy  
both, frequency nadir and RoCoF standards, the lower bound  
for virtual inertia in the optimization problem and for each area  
are selected as the maximum value of (21) and (25), namely:

$$h_{i,min} = \max \{ h'_{i,min}, h''_{i,min} \} \quad (26)$$

Moreover, the overall system inertia has a direct impact on the  
frequency indices. This means that some considerations should  
be made regarding overall system inertia and, consequently,  
(21) and (25) would be completed by adding a new equality  
constraint. For this purpose, the frequency of the overall Center  
of Inertia (COI), which should satisfy strict frequency standards,  
would be employed to determine the overall amount of inertia  
in the system, as [5]:

$$H_{COI} = Q = H \frac{\Delta f_{COI}}{f_{COI}} (61.5) \quad (27)$$

where,  $\Delta f_{COI}$ , and  $f_{COI}$  represent the frequency deviation and  
frequency of the system, without ESS, after the fault, respec-  
tively. Formally, equation (27) gives the required amount of iner-  
tia constant which guarantees acceptable frequency dynamics of  
the COI. Of note that  $Q$  would be realized by adding the emulated  
inertia of ESSs to the conventional SGs inertia. Accordingly, the  
optimization problem (15) can be re-written as:

$$\text{minimize}_{h_i} F(h_i) = \sum_{i=1}^{n_{ESS}} \left( C_{LCC,a} \frac{h_i S_{base}}{3600 \text{ sec}} \right) \quad (28.a)$$

$$\text{st: } H_{COI} = Q \quad (28.b)$$

$$h_{i,min} \leq h_i \leq h_{i,max} \quad (28.c)$$

$$SOC_{min} \leq SOC_i \leq SOC_{max} \quad (28.d)$$

where the dynamic inequality constraints (15.b) and (15.c) are  
re-formulated as the algebraic inequality constraint (28.c) in  
terms of the inertia constant. This dramatically increases the  
simplicity and speed of the calculations.

#### IV. SOLUTION ALGORITHM

In this section, a framework that incorporates the model (6)  
and the objective function (28) to optimally place battery ESS  
in the system is proposed.

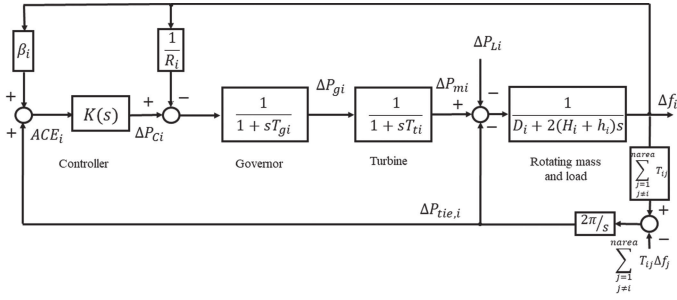


Fig. 6. Block diagram representation of control area  $i$ .  $\beta_i$ ,  $R_i$ ,  $T_{gi}$ ,  $T_{ti}$ , and  $D_i$  are frequency bias, droop characteristic, governor time constant, turbine time constant, and damping property, respectively.

439 The algorithm consists of 4 main steps:

- 440 *Step 1:* Define PV buses of the system as candidates for battery  
 441 ESSs placement;  
 442 *Step 2:* Assume the proposed model (6), with unknown inertia  
 443 constant, in each PV bus;  
 444 *Step 3:* Define the emulated inertia constant, i.e.  $h$ , as a decision  
 445 variable of the objective function (28). Set  $C$  in (6) as the  
 446 product of the ratio of  $h$  to the inertia constant of the installed  
 447 SG, in the associated bus, and the mechanical power of the  
 448 SG;  
 449 *Step 4:* Apply a Genetic Algorithm (GA) to solve the minimiza-  
 450 tion problem (28). Indeed, the GA determines the amount of  
 451 virtual inertia in each PV bus of the system.

## 452 V. SIMULATION AND RESULTS

453 Three test systems have been used for evaluating the proposed  
 454 formulation in this paper: a) a linearized model of a three-area  
 455 power system, b) a nonlinear yet simple two-area, four-machine  
 456 test system, and c) a large scale 16-machine, five-area 68-bus test  
 457 model of the New York/New England system.

### 458 A. Linear System

459 As a first motivating example, a linearized model of a three-  
 460 area power system is used to assess the efficiency of the proposed  
 461 formulation. The block diagram of each area is shown in Fig. 6.

462 Firstly, a 0.2 per unit load disturbance is applied at areas 1  
 463 and 3. As a first scenario, the required virtual inertia is calculated  
 464 only based on (28.b) and arbitrary realized, through the proposed  
 465 model in (6), in area 1. For simulation purposes, it is assumed  
 466 that the ESS would be triggered upon occurrence of the fault.  
 467 Comparison of frequency dynamics for the system with and  
 468 without virtual inertia reveals that while areas 1 and 2 frequency  
 469 nadirs improved by means of virtual inertia, area 3 shows an  
 470 undesired behavior. This in turn numerically justifies the need  
 471 for optimal inertia placement. Within this framework, (28) may  
 472 be written as:

$$473 \underset{h_i}{\text{minimize}} \quad F(h_i) = \sum_{i=1}^{n_{ESS}} \left( C_{LCC,a i} \frac{h_i S_{base}}{3600 \text{ sec}} \right) \quad (29.a)$$

$$474 \text{st:} \quad H_{COI} = 0.053 \quad (29.b)$$

TABLE I  
OPTIMIZATION RESULTS IN THREE AREA SYSTEM

Method	$h_1$	$h_2$	$h_3$	$F(h_i)$
PM*	0.016	0	0.037	2.5916
Ref. [2]	0.023	0.016	0.022	3.0942
Ref. [44]	0.012	0.009	0.038	2.8735

a.PM: Proposed Method

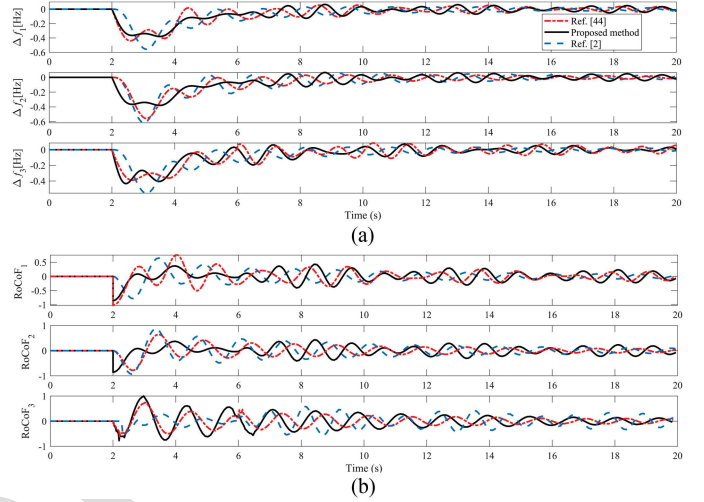


Fig. 7. (a) Frequency behaviors and (b) RoCoF of generators 1, through 3 of three area power system for three cases: proposed formulation, Ref. [44] and Ref. [2].

$$0.0129 \leq h_1 \quad (29.c)$$

$$0 \leq h_2 \quad (29.d)$$

$$0.0225 \leq h_3 \quad (29.e)$$

$$30\% \leq SOC_i \leq 80\% \quad (29.f)$$

475 where, for instance, the minimum inertia of area 1 in (29.c) is  
 476 calculated based on (21),(25), and (26) as:

$$h'_{1,\min} = 0.08335 \times \left( \frac{-1 + 1.1870}{-1.1870} \right) = 0.0129$$

$$h''_{1,\min} = 0$$

$$h_{1,\min} = \max \{0, 0.0129\} = 0.0129 \quad (30)$$

477 Note that some other unspecified parameters of (29) would  
 478 be set as described in Appendix A. The results obtained, using  
 479 a simple GA with 0.05 and 0.8 mutation and crossover coef-  
 480 ficients, respectively, from optimization of (29) are shown in  
 481 Table I. In order to further assess efficiency of the proposed  
 482 formulation, Table I compares the results with those of ob-  
 483 tained from [2] and [44]. Comparison results justify the fact  
 484 that dynamic behavior of ESS could significantly affect optimal  
 485 placement problem which is missed in previous research.

486 Figure 7 compares the frequency behavior and RoCoF of  
 487 generators 1, 2 through 3 for three cases of interest: a) with  
 488 virtual inertia and according to the proposed formulation, b) with  
 489 virtual inertia and according to [44], and c) with virtual inertia  
 490 and according to [2]. It can be seen that while frequency traces



TABLE II  
MODAL ANALYSIS OF THE SYSTEMS WITH VI

Method	PM	Ref. [2]	Ref. [44]
Damping	0.2762	0.1265	0.2634

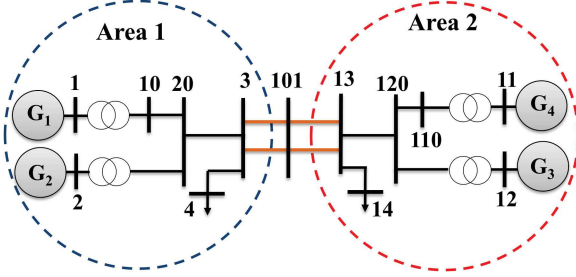


Fig. 8. Single-line diagram of two area system.

of [2], [44] and the proposed method in this paper follow the standards regarding RoCoF and frequency nadir, the proposed formulation results in less ESS capacity.

Also of interest, modal analysis of the results, as explained in Table II, shows the efficiency of the proposed formulation in comparison with that of [2] and [44].

Results show that a lower emulated virtual inertia in the proposed formulation not only decreases the cost function but also causes better performance in terms of enhanced damping.

With virtual inertia, the results from [2] and [44] also seem to perform within the constraints and are almost the same as the results from the proposed method. This could be justified through the fact that set of PV buses for small systems includes a few members to be considered as candidates of ESS installation. Therefore, different algorithms may differ a bit from capacity point of view rather than location which in turn causes negligible difference between the results. To further assess simultaneous effects of virtual inertia on frequency and transient stabilities, two non-linear system are used in what follows.

### B. Two-Area Power System

The two-area power system, shown in Fig. 8, is considered to further demonstrate the efficiency of the proposed formulation. Modeling considerations are essentially those described in [45]; all the generating units are modeled with 6<sup>th</sup> order synchronous machine models with excitation systems.

The disturbance of interest is the outage of generator  $G_4$ , at the first second of simulation. The lower bounds of virtual inertia are calculated according to (29) and (30) as:

$$\underset{h_i}{\text{minimize}} \quad F(h_i) = \sum_{i=1}^{n_{ESS}} \left( C_{LCC,a} i \frac{h_i S_{base}}{3600 \text{ sec}} \right) \quad (31.a)$$

$$\text{st :} \quad H_{COI} = 4.973 \quad (31.b)$$

$$0.3151 \leq h_1$$

$$0.3881 \leq h_2$$

$$0 \leq h_3$$

$$30\% \leq SOC_i \leq 80\% \quad (31.c)$$

TABLE III  
OPTIMIZATION RESULTS IN TWO AREA SYSTEM

Method	$h1$	$h2$	$h3$	$F(h_i)$
PM	0.402	0.567	0.004	4.6705
Ref. [2]	0.116	0.332	0.376	6.3104
Ref. [44]	0.212	0.315	0.316	5.7891

TABLE IV  
FREQUENCY INDICATORS OF TWO AREA SYSTEM BEFORE AND AFTER APPLICATION OF OPTIMAL INERTIA VALUES

$G_i$	Without VI		With VI (PM)		With VI [2]		With VI [44]	
	RoCoF (Hz/s)	$\Delta f_{nadir}$ (Hz)	RoCoF (Hz/s)	$\Delta f_{nadir}$ (Hz)	RoCoF (Hz/s)	$\Delta f_{nadir}$ (Hz)	RoCoF (Hz/s)	$\Delta f_{nadir}$ (Hz)
1	1.187	0.172	0.989	0.143	0.988	0.126	0.973	0.116
2	1.240	0.160	0.989	0.134	0.981	0.112	0.961	0.162
3	0.706	0.267	0.713	0.254	0.730	0.200	0.786	0.198

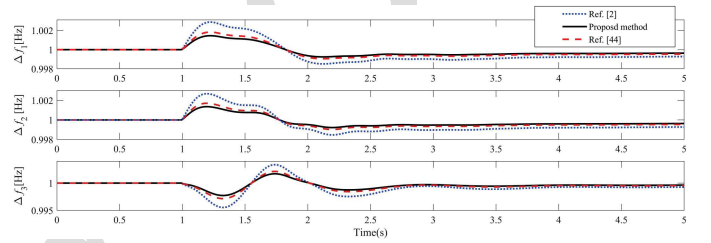


Fig. 9. Frequency response of generators 1, 2 and 3 of the two area power system for three cases: proposed formulation, Ref. [44] and Ref. [2].

in which, equality constraint of (31.b) reveals:

$$H_{COI} + h_{ESS} = 4.973 \rightarrow h_{ESS} = 4.973 - 4 = 0.973 \quad (32)$$

Solving (28) leads to the optimum results of Table III. The results also compared with those of optimum virtual inertia of [2] and [44].

Further, Table IV compares frequency stability indices for different approaches. The results demonstrate high efficiency of the proposed method to optimally allocate virtual inertia in the system.

While the frequency nadir of the generators are within the permissible range for the system without virtual inertia, the RoCoFs for the generators 1 and 2 exceed the standard value. Optimal placement of virtual inertia returns generators with undesired frequency dynamics to the normal region. Efficiency of the proposed method is further assessed through time domain simulations of Fig. 9.

Also of interest, effects of virtual inertia on transient stability is assessed using a simple power angle-based stability index  $\eta$  [18]:

$$\eta = \frac{360 - \delta_{max}}{360 + \delta_{max}} \quad (33)$$

where  $\delta_{max}$  is the maximum angle separation between any two generators in the system [46]. Generally stated, the use of simple metrics such as (33) may work for some systems but fail for some others. During severe faults, most ESSs, if remain connected and continue to inject active power which is not the case in many regions, get saturated and cannot follow the frequency properly. Using (33) in this paper relies on a conservative assumption that

TABLE V  
 TRANSIENTS STABILITY ASSESSMENT

Method	$\delta_{max}$	$\eta$
PM	11.02	0.94
Ref. [2]	20.8	0.89
Ref. [44]	16.63	0.91

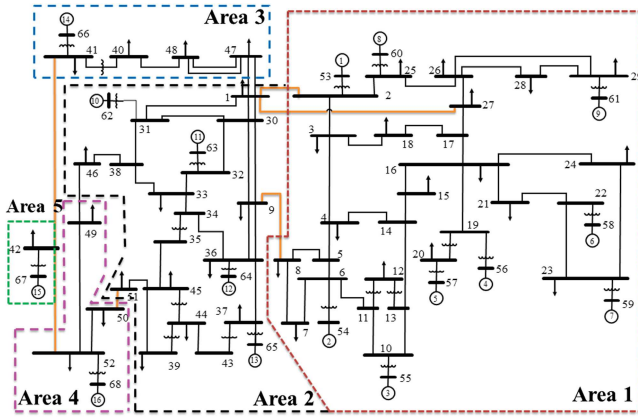


Fig. 10. Single line diagram of the 68-bus system showing coherent areas and their interconnections.

542 the occurred fault is not a severe one, which causes ESSs to  
 543 be disconnected from the grid. Moreover, saturation of ESSs  
 544 in response to sever faults is neglected. Table V demonstrates  
 545 better performance of the proposed method in comparison with  
 546 those of [2] and [44].

547 Note in these results, that a higher value of \*\*\* corresponds to  
 548 a more favorable transient stability condition.

### 549 C. New York/New England System

550 The New England test system is used to further illustrate  
 551 the efficiency of the proposed algorithm for large scale power  
 552 systems. A single-line diagram of the system, showing major  
 553 coherent areas and their interconnections, is shown in Fig. 10.

554 Five different contingency scenarios, including tripping of  
 555 major generating units and load shedding, are considered. Results  
 556 in Table VI compare the proposed algorithm results with those of [2]  
 557 and [44]. The results show high efficiency of the proposed method  
 558 to improve frequency dynamics with minimum  
 559 cost.

560 Also of interest, Fig. 11 shows the allocation of virtual inertia  
 561 among the PV buses of the system.

562 Moreover, Fig. 12 compares the frequency behavior of the  
 563 system, in response to the outage of generator n1 (scenario  
 564 1), for the proposed method, [2] and [44]. It should be noted  
 565 that while there are negligible deviations between the traces in  
 566 Fig. 12, significant differences between the cost functions justify  
 567 the efficiency of the proposed method.

568 Results show that the optimization problem works better  
 569 and more effectively for larger areas. This can be understood  
 570 by noting that set of PV buses for large areas includes many  
 571 members to be considered as candidates for ESS placement.  
 572 As a result, there are a lot of possibilities for both the size and  
 573 location.

 TABLE VI  
 OPTIMIZATION RESULTS IN NEW YORK/NEW ENGLAND SYSTEM

		$h_1$	$h_2$	$h_3$	$h_4$	$h_5$	$F(h_i)$
1	PM	0.412	0.432	0.313	0.092	0.111	9.2141
	Ref. [2]	0.506	0.332	0.376	0.201	0.112	12.4031
	Ref. [44]	0.378	0.453	0.306	0.115	0.098	11.0817
2	PM	0.341	0.513	0.209	0.101	0.098	10.8601
	Ref. [2]	0.340	0.712	0.301	0.113	0.160	13.0012
	Ref. [44]	0.300	0.798	0.251	0.098	0.161	12.3140
3	PM	0.474	0.261	0.160	0.261	0.007	9.7516
	Ref. [2]	0.596	0.298	0.267	0.271	0.088	11.2113
	Ref. [44]	0.314	0.351	0.294	0.314	~0	10.0087
4	PM	0.169	0.203	0.617	0.135	0.072	9.8617
	Ref. [2]	0.132	0.512	0.694	0.196	0.209	10.5103
	Ref. [44]	0.100	0.374	0.687	0.096	0.101	10.0102
5	PM	0.613	0.032	0.116	0.076	~0	9.0412
	Ref. [2]	0.743	0.215	0.402	0.031	~0	9.9731
	Ref. [44]	0.412	0.354	0.391	0.116	~0	9.4019

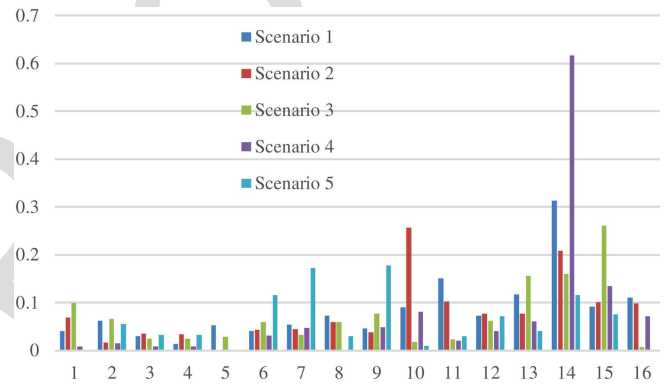


Fig. 11. Virtual inertia allocation for New-England system.

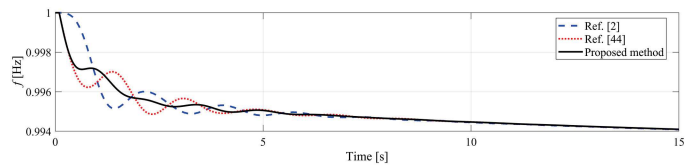


Fig. 12. Frequency responses of New England system for different approaches.

574 Moreover, the efficiency of the proposed formulation to enhance  
 575 transient stability is shown in Table VII, using (33).

576 Table VII shows that appropriate placement of virtual inertia  
 577 in the system, considering dynamical behavior of ESS, could  
 578 also improve transient stability. This could be justified through  
 579 the fact that the so far researches, e.g. [2], rely on quasi-steady  
 580 state phasors for voltages and currents in transient stability  
 581 assessment. In other words, they consider constant nominal  
 582 value of frequency in defining system impedances which is far  
 583 from realistic for system with penetration of inverter based  
 584 ESSs. This point is successfully addressed in the proposed  
 585 formulation by explicitly representing the dynamic behavior of  
 586 ESSs in the problem formulation.

TABLE VII  
OPTIMIZATION RESULTS IN NEW ENGLAND SYSTEM

Method	$\eta_{12}$	$\eta_{13}$	$\eta_{14}$	$\eta_{15}$	$\eta_{25}$	$\eta_{35}$
PM	0.92	0.87	0.91	0.89	0.90	0.89
1 Ref. [2]	0.85	0.84	0.91	0.90	0.85	0.87
Ref. [44]	0.87	0.86	0.91	0.89	0.88	0.88
PM	0.98	0.83	0.92	0.93	0.95	0.95
2 Ref. [44]	0.94	0.82	0.91	0.90	0.91	0.92
Ref. [2]	0.91	0.84	0.90	0.88	0.89	0.95
PM	0.87	0.90	0.90	0.89	0.92	0.92
3 Ref. [44]	0.85	0.88	0.90	0.88	0.88	0.88
Ref. [2]	0.88	0.85	0.87	0.87	0.87	0.88
PM	0.96	0.93	0.93	0.93	0.93	0.93
4 Ref. [44]	0.96	0.90	0.91	0.93	0.92	0.89
Ref. [2]	0.95	0.94	0.93	0.93	0.91	0.85
PM	0.94	0.85	0.92	0.92	0.91	0.96
5 Ref. [44]	0.89	0.86	0.90	0.90	0.89	0.94
Ref. [2]	0.93	0.87	0.87	0.87	0.88	0.91

## VI. SENSITIVITY AND UNCERTAINTY ANALYSIS

In this section, sensitivity analyses are conducted to understand the effect of operation conditions, including variations of faults magnitude, operating point, and annualized LCC on the optimization problem. For this purpose, (28.a) is used to calculate sensitivity of the cost function to operation condition, as:

$$F(h_i) + \Delta F(h_i) = \sum_{i=1}^{n_{ESS}} \left( C_{LCC,a,i} \frac{h_i S_{base}}{3600 \text{ sec}} \right) + \frac{\partial F(h_i)}{\partial \Delta P_L} \Delta \Delta P_L + \frac{\partial F(h_i)}{\partial \Delta P_m} \Delta \Delta P_m + \frac{\partial F(h_i)}{\partial C_{LCC,a,i}} \Delta C_{LCC,a,i} \quad (34)$$

Then, according to (19) and (23), one could write the sensitivity matrix (26) as:

$$\begin{bmatrix} \partial h'_{i,\min} \\ \partial h''_{i,\min} \end{bmatrix} = \begin{bmatrix} \frac{\partial RoCoF_i}{\partial \Delta P_{Li}} & \frac{\partial RoCoF_i}{\partial \Delta P_{mi}} \\ \frac{\partial \Delta f_{nadir,i}}{\partial \Delta P_{Li}} & 0 \end{bmatrix} \begin{bmatrix} \Delta \Delta P_{Li} \\ \Delta \Delta P_{mi} \end{bmatrix} \quad (35)$$

Considering (35) in (34) gives:

$$\begin{aligned} \Delta F(h_i) &= \frac{\partial F(h_i)}{\partial h_i} \frac{\partial h_i}{\partial \Delta P_L} \Delta \Delta P_L + \frac{\partial F(h_i)}{\partial h_i} \frac{\partial h_i}{\partial \Delta P_m} \Delta \Delta P_m \\ &= \sum_{i=1}^{n_{ESS}} \left( C_{LCC,a,i} \frac{S_{base}}{3600 \text{ sec}} \right) \times \max \left\{ \frac{\partial RoCoF_i}{\partial \Delta P_{Li}} \Delta \Delta P_L \right. \\ &\quad \left. + \frac{\partial RoCoF_i}{\partial \Delta P_{mi}} \Delta \Delta P_m, \frac{\partial \Delta f_{nadir,i}}{\partial \Delta P_{Li}} \Delta \Delta P_{Li} \right\} \\ &\quad + \sum_{i=1}^{n_{ESS}} \left( \frac{h_i S_{base}}{3600 \text{ sec}} \right) \Delta C_{LCC,a,i} \quad (36) \end{aligned}$$

The usefulness of (36) is now assessed for the New-England system. For this purpose, contingency 1, i.e. the outage of generator 1 in area 1, is considered as the base case. Cost function for outage of generator 7 in area 1, i.e. scenario 2, and generator 11 in area 2, i.e. scenario 3, are calculated using (36). Table VIII

TABLE VIII  
SENSITIVITY ANALYSIS

Scenario	Cost function of (28)	Cost function of (35)
2	9.7516	9.5913
3	9.8617	9.9302

compares the results which clearly justify effectiveness of the proposed sensitivity analysis.

For uncertainty analysis, the equality constraint of (28.b) is represented in the objective function (28.a), as:

$$\begin{aligned} \underset{h_i}{\text{minimize}} \quad F(h_i) &= \sum_{i=1}^{n_{ESS}} \left( C_{LCC,a,i} \frac{h_i S_{base}}{3600 \text{ sec}} \right) \\ &\quad + \beta(H_{COI} - Q) \quad (37) \end{aligned}$$

where  $b$  is arbitrary chosen high with the aim of enforcing the results to follow the equality constraint of (28.b). Considering parametric uncertainty for inertia constant i.e.  $H_{COI}$ , one could write (37) as:

$$\begin{aligned} \underset{h_i}{\text{minimize}} \quad F(h_i) &= \sum_{i=1}^{n_{ESS}} \left( C_{LCC,a,i} \frac{h_i S_{base}}{3600 \text{ sec}} \right) \\ &\quad + \beta(H_{COI} + \gamma - Q) \rightarrow \\ \underset{h_i}{\text{minimize}} \quad F(h_i) &= \sum_{i=1}^{n_{ESS}} \left( C_{LCC,a,i} \frac{h_i S_{base}}{3600 \text{ sec}} \right) \\ &\quad + \beta(H_{COI} - Q) + \beta\gamma \quad (38) \end{aligned}$$

where  $g$  expressed in percentage of  $H_{COI}$ . To deal with uncertainty analysis, a simple interval approach is utilized. It assumes that the uncertain parameters take value in a specified interval. It could be reinterpreted as the probabilistic modeling with a uniform probability density function (PDF). In this method, the upper and lower bounds for the uncertain inertia parameter are defined. The aim is to find the lower and upper bounds of objective function [47].

Using the proposed framework, assume that the maximum uncertainty of inertia constant is considered to be 5p. This means that the interval of interest can be defined as:

$$\gamma = [H_{COI} - 0.05(H_{COI}), H_{COI} + 0.05(H_{COI})] \quad (39)$$

which in turn causes  $F(h_i)$  as:

$$F(h_i) = [3.8298, 5.5112] \quad (40)$$

with a uniform PDF.

## VII. CONCLUSION

While rotational inertia stabilizes the frequency of power grids against small and large disturbances, it leads for oscillations between generators. This paper provides a framework for optimal placement of virtual inertia in low inertia power systems which in turn improves host grid frequency stability. In this way, the ESSs are used to emulate virtual inertia placement. On the other hand, the proposed method in this paper tackles dynamical behavior of the ESSs into problem formulation and

thus causes less, in comparison with the literature, virtual inertia to be implemented in the system. This in turn causes better rotor angle stability features. Of note that the proposed algorithm can be a valuable tool in generation expansion planning of power system and inertia deployment.

A data driven-based approach to represent the ESS dynamics using conventional synchronous generator is proposed. This in turn causes the gathered data, from the field setup, provides complementary information to the conventional based model of synchronous generator. Simulation results validate accuracy and efficiency of the proposed modelling procedure.

Using the proposed strategy in a linear three-area power system and two non-linear systems, the required ESS for each area with the lowest cost and capacity are determined. It was found that the calculated values could well maintain the frequency indices within the permissible range. Also, the results showed that the optimal virtual inertia arrangement could have a positive effect on the transient stability and the amount of power exchange between control areas.

## APPENDIX

TABLE IX  
ECONOMICAL PARAMETERS RELATED TO THE OPTIMIZATION PROBLEM [25], [26]

Parameter	Value	Parameter	Value
$i(\%)$	8	$C_{FOM,a} (\$/kw\text{-yr})$	10
$C_{PSC} (\$/kw)$	200	$C_{VOM,a} (\$/kwh)$	5
$C_{BOP} (\$/kw)$	50	$R$	2
$C_{stop} (\$/kw)$	300	$t(\text{yr})$	6
$C_R (\$/kw)$	300	$\eta_{sys}(\%)$	75

TABLE X  
TECHNICAL PARAMETERS RELATED TO THE OPTIMIZATION PROBLEM [22], [24].

Parameter	Value	Parameter	Value
$S_{base} (MVA)$	1000	$P_{ESS} (MW)$	1
$RoCoF_{max} (Hz/s)$	1	$E_{ESS, rated} (MVAh)$	0.25
$\Delta f_{nadir, max} (Hz)$	0.8	$\eta_a^+ \eta_c(\%)$	75
$SOC(0)$	0.5	$t(\text{yr})$	15
$SOC_{min}$	0.3	$t_{ch}(\text{hrs})$	0.25
$SOC_{max}$	0.8	$n_{cycle}$	1000

## REFERENCES

- [1] A. Mullane and M. O'Malley, "The inertial response of induction-machine-based wind turbines," *IEEE Trans. Power Syst.*, vol. 20, no. 3, pp. 1496–1503, Aug. 2005.
- [2] B. K. Poolla, S. Bolognani, and F. Dörfler, "Optimal placement of virtual inertia in power grids," *IEEE Trans. Autom. Control*, vol. 62, no. 12, pp. 6209–6220, 2017.
- [3] H. Bevrani, B. François, and T. Ise, *Microgrid dynamics and control*. Hoboken, NJ, USA: John Wiley & Sons, 2017.
- [4] H. Golpíra and A. R. Messina, "A center-of-gravity-based approach to estimate slow power and frequency variations," *IEEE Trans. Power Syst.*, vol. 33, no. 1, pp. 1026–1035, Jan. 2018.
- [5] B. Lian, A. Sims, D. Yu, C. Wang, and R. W. Dunn, "Optimizing LiFePO4 battery energy storage systems for frequency response in the UK system," *IEEE Trans. Sustain. Energy*, vol. 8, no. 1, pp. 385–394, Jan. 2017.
- [6] Z. Wu, D. W. Gao, H. Zhang, S. Yan, and X. Wang, "Coordinated control strategy of battery energy storage system and PMSG-WTG to enhance system frequency regulation capability," *IEEE Trans. Sustain. Energy*, vol. 8, no. 3, pp. 1330–1343, Jul. 2017.
- [7] F. Zhang, Z. Hu, X. Xie, J. Zhang, and Y. Song, "Assessment of the effectiveness of energy storage resources in the frequency regulation of a single-area power system," *IEEE Trans. Power Syst.*, vol. 32, no. 5, pp. 3373–3380, Sep. 2017.
- [8] A. S. Ahmadyar, S. Riaz, G. Verbič, A. Chapman, and D. J. Hill, "A framework for assessing renewable integration limits with respect to frequency performance," *IEEE Trans. Power Syst.*, vol. 33, no. 4, pp. 4444–4453, Jul. 2018.
- [9] H. Golpíra, H. Seifi, A. R. Messina, and M.-R. Haghifam, "Maximum penetration level of micro-grids in large-scale power systems: Frequency stability viewpoint," *IEEE Trans. Power Syst.*, vol. 31, no. 6, pp. 5163–5171, Nov. 2016.
- [10] E. Spahic, D. Varma, G. Beck, G. Kuhn, and V. Hild, "Impact of reduced system inertia on stable power system operation and an overview of possible solutions," in *Proc. IEEE Power Energy Soc. Gen. Meet.*, 2016, pp. 1–5.
- [11] A. Ulbig, T. S. Borsche, and G. Andersson, "Impact of low rotational inertia on power system stability and operation," *Int. Federation Accountants Proc. Vol.*, vol. 47, no. 3, pp. 7290–7297, 2014.
- [12] Y. Wang, H. Bayem, M. Giralt-Devant, V. Silva, X. Guillaud, and B. Francois, "Methods for assessing available wind primary power reserve," *IEEE Trans. Sustain. Energy* vol. 6, no. 1, pp. 272–280, Jan. 2015.
- [13] Y. Wang, G. Delille, H. Bayem, X. Guillaud, and B. Francois, "High wind power penetration in isolated power systems—Assessment of wind inertial and primary frequency responses," *IEEE Trans. Power Syst.*, vol. 28, no. 3, pp. 2412–2420, Aug. 2013.
- [14] Z. Chu, U. Markovic, G. Hug, and F. Teng, "Towards optimal system scheduling with synthetic inertia provision from wind turbines," *IEEE Trans. Power Syst.* to be published, 2020.
- [15] H. Golpíra, A. R. Messina, and H. Bevrani, "Emulation of virtual inertia to accommodate higher penetration levels of distributed generation in power grids," *IEEE Trans. Power Syst.*, vol. 34, no. 5, pp. 3384–3394, Sep. 2019.
- [16] S. D'Arco and J. A. Suul, "Equivalence of virtual synchronous machines and frequency-droops for converter-based microgrids," *IEEE Trans. Smart Grid*, vol. 5, no. 1, pp. 394–395, Jan. 2014.
- [17] E. Rakhshani, D. Remon, A. M. Cantarellas, and P. Rodriguez, "Analysis of derivative control based virtual inertia in multi-area high-voltage direct current interconnected power systems," *IET Gener. Transmiss. Distribution*, vol. 10, no. 6, pp. 1458–1469, 2016.
- [18] E. Hammad, A. Farraj, and D. Kundur, "On effective virtual inertia of storage-based distributed control for transient stability," *IEEE Trans. Smart Grid*, vol. 10, no. 1, pp. 327–336, Jan. 2019.
- [19] W. J. Farmer and A. Rix, "Optimising power system frequency stability using virtual inertia from inverter-based renewable energy generation," in *Proc. Int. Conf. Clean Electr. Power*, 2019, pp. 394–404.
- [20] A. Attya, O. Anaya-Lara, and W. Leithead, "Novel concept of renewables association with synchronous generation for enhancing the provision of ancillary services," *Appl. Energy*, vol. 229, pp. 1035–1047, 2018.
- [21] B. K. Poolla, D. Groß, and F. Dörfler, "Placement and implementation of grid-forming and grid-following virtual inertia and fast frequency response," *IEEE Trans. Power Syst.*, vol. 34, no. 4, pp. 3035–3046, Jul. 2019.
- [22] T. S. Borsche, T. Liu, and D. J. Hill, "Effects of rotational inertia on power system damping and frequency transients," in *54th IEEE Conf. Decis. Control*, 2015, IEEE, pp. 5940–5946.
- [23] M. H. Fini and M. E. H. Golshan, "Determining optimal virtual inertia and frequency control parameters to preserve the frequency stability in islanded microgrids with high penetration of renewables," *Electr. Power Syst. Res.*, vol. 154, pp. 13–22, 2018.
- [24] A. Oudalov, D. Chartouni, and C. Ohler, "Optimizing a battery energy storage system for primary frequency control," *IEEE Trans. Power Syst.*, vol. 22, no. 3, pp. 1259–1266, Aug. 2007.
- [25] S. Wogrin and D. F. Gayme, "Optimizing storage siting, sizing, and technology portfolios in transmission-constrained networks," *IEEE Trans. Power Syst.*, vol. 30, no. 6, pp. 3304–3313, Nov. 2015.
- [26] O. Mo, S. D'Arco, and J. A. Suul, "Evaluation of virtual synchronous machines with dynamic or quasi-stationary machine models," *IEEE Trans. Ind. Electron.*, vol. 64, no. 7, pp. 5952–5962, Jul. 2017.
- [27] O. Ajala, A. Dominguez-garcia, P. Sauer, and D. Liberzon, "A library of second-order models for synchronous machines," 2018, *arXiv:1803.09707*.
- [28] M. H. Bollen and I. Y. Gu, *Signal Processing of Power Quality Disturbances*. Hoboken, NJ, USA: John Wiley & Sons, 2006.
- [29] D. G. Manolakis, V. K. Ingle, and S. M. Kogon, *Statistical and Adaptive Signal Processing: Spectral Estimation, Signal Modeling, Adaptive Filtering, and Array Processing*. New York, NY, USA: McGraw-Hill, 2000.

651

652

653

654

655

656

657

658

659

660

661

662

663

664

665

666

667

668

669

670

671

672

673

674

675

676

677

678

679

680

681

682

683

684

685

686

687

688

689

690

691

692

693

694

695

696

697

698

699

700

701

702

703

704

705

706

707

708

709

710

711

712

713

714

715

716

717

718

719

720

721

722

723

724

725

726

727

728

729

730

731

732

733

734

735

736

737

738

739

740

741

742

743

744

745

Q4

Q5

- 746 [30] H. Golpîra, "Bulk power system frequency stability assessment in presence of microgrids," *Electric Power Syst. Res.*, vol. 174, 2019, Art. no. 105863. 771
- 747 [31] B. Zakeri and S. Syri, "Electrical energy storage systems: A comparative 772
- 748 life cycle cost analysis," *Renewable Sustain. Energy Rev.*, vol. 42, pp. 569– 773
- 749 596, 2015. 774
- 750 [32] K. Mongird *et al.*, "Energy storage technology and cost characterization 775
- 751 report," *Pacific Northwest National Lab.(PNNL)*. Richland, WA (United 776
- 752 States), 2019. 777
- Q6 753 [33] *Fast Freq. Response Concepts Bulk Power Syst. Rel. Needs*, NERC, 2020. 778
- Q7 754 [34] I. Teruo, "State of charge calculation device and state of charge calculation 779
- 755 method," ed: US Patents, US6845332B2, 2005. 780
- 756 [35] Z. X. Tang and Y. S. Lim, "Frequency regulation mechanism of energy 781
- 757 storage system for the power grid," in *Proc. 4th IET Clean Energy Technol. 782*
- Q8 758 *Conf.*, 2016. 783
- 759 [36] J. H. Eto, "Use of frequency response metrics to assess the planning 784
- 760 and operating requirements for reliable integration of variable renewable 785
- 761 generation," *Ernest Orlando Lawrence Berkeley National Laboratory*. 786
- 762 Berkeley, CA: Tech. Rep. LBNL-4142E, 2011. 787
- 763 [37] *Frequency Stability Evaluation Criteria for the Synchronous Zone of 788*
- 764 *Continental Europe –Requirements and impacting factors*. Brussels, Bel- 789
- 765 gium: European Network of Transmission System Operators for Electricity 790
- 766 (entsoe), 2016. 791
- 767 [38] Y. Wen, W. Li, G. Huang, and X. Liu, "Frequency dynamics constrained 792
- 768 unit commitment with battery energy storage," *IEEE Trans. Power Syst.*, 793
- 769 vol. 31, no. 6, pp. 5115–5125, Nov. 2016.
- [39] A. Ekwue and B. Cory, "Transmission system expansion planning by 771
- 772 interactive methods," *IEEE Trans. Power App. Syst.*, no. 7, pp. 1583–1591, 773
- 774 Jul. 1984. 775
- [40] C. E. O. H. ENTSO-E, "P1-Policy 1: Load-frequency control and perfor- 776
- 777 mance," ed: Tech. Rep. 2000-130-003, May 2000. 778
- [41] H. Chavez, R. Baldick, and S. Sharma, "Governor rate-constrained OPF 779
- 780 for primary frequency control adequacy," *IEEE Trans. Power Syst.*, vol. 29, 781
- 782 no. 3, pp. 1473–1480, May 2014. 783
- [42] F. Teng, V. Trovato, and G. Strbac, "Stochastic scheduling with inertia- 784
- 785 dependent fast frequency response requirements," *IEEE Trans. Power 786*
- 787 *Syst.*, vol. 31, no. 2, pp. 1557–1566, Mar. 2016. 788
- [43] N. Grid. "Security and quality of supply standards," [Online] Available: 789
- 790 [http://www2.nationalgrid.com/UK/Industry-information/Electricity-](http://www2.nationalgrid.com/UK/Industry-information/Electricity-codes/System-Security-and-Quality-of-Supply-Standards/) 791
- 792 [codes/System-Security-and-Quality-of-Supply-Standards/](http://www2.nationalgrid.com/UK/Industry-information/Electricity-codes/System-Security-and-Quality-of-Supply-Standards/) 793
- 794 [44] T. Borsche and F. Dörfler, "On placement of synthetic inertia with explicit 795
- 796 time-domain constraints," 2017, *arXiv:1705.03244*. 797
- [45] G. Rogers, *Power System Oscillations*. Berlin, Germany: Springer Science 798
- 799 a Business Media, 2012. 800
- [46] P. L. Inc and TSAT, "Transient security assessment tool user manual," 801
- 802 Powertech Labs Inc. 803
- [47] M. Aien, A. Hajebrahimi, and M. Fotuhi-Firuzabad, "A comprehensive 804
- 805 review on uncertainty modeling techniques in power system studies," 806
- 807 *Renewable Sustain. Energy Rev.*, vol. 57, pp. 1077–1089, 2016. 808
- 809